PCCP

PAPER

View Article Online
View Journal | View Issue

Cite this: *Phys. Chem. Chem. Phys.*, 2021, **23**, 11672

Fracto-eutectogels: SDS fractal dendrites *via* counterion condensation in a deep eutectic solvent†

Lauren Matthews, ‡[ab] Silvia Ruscigno,[a] Sarah E. Rogers,[c] Paul Bartlett,[a] Andrew J. Johnson,[d] Robert Sochon[d] and Wuge H. Briscoe *[a]

Glyceline, a deep eutectic solvent comprising glycerol and choline chloride, is a green nonaqueous solvent with potential industrial applications. Molecular mechanisms of surfactant self-assembly in deep eutectic solvents are expected to differ from those in their constituent polar components and are not well understood. Here we report the observation of self-assembled SDS fractal dendrites with dimensions up to ~mm in glyceline at SDS concentrations as low as c_{SDS} ~ 0.1 wt%. The prevalence of these dendritic fractal aggregates led to the formation of a gel phase at SDS concentrations above ≥1.9 wt% (the critical gelation concentration c_{CGC}). The gel microscopic structure was visualised using polarised light microscopy (PLM); rheology measurements confirmed the formation of a colloidal gel, where the first normal stress difference was negative and the elastic modulus was dominant. Detailed nano-structural characterisation by small-angle neutron scattering (SANS) further confirmed the presence of fractal aggregates. Such SDS aggregation or gelation has not been observed in water at such low surfactant concentrations, whereas SDS has been reported to form lamellar aggregates in glycerol (a component of glyceline). We attribute the formation of the SDS fractal dendrites to the condensation of counterions (*i.e.* the choline ions) around the SDS aggregates – a diffusion-controlled process, leading to the aggregate morphology observed. These unprecedented results shed light on the molecular mechanisms of surfactant self-assembly in deep eutectic solvents, important to their application in industrial formulation.

Received 29th March 2021,
Accepted 4th May 2021

DOI: 10.1039/d1cp01370j

rsc.li/pccp

1. Introduction

Deep eutectic solvents (DES)[1,2] are green, non-volatile, and they are good solvents for many inorganic and organic species.[3,4] Their green credentials are of interest in many industrial applications ranging from electroplating[5–9] to personal care products. DES have also been shown to improve rates and enantioselectivities of lipase-catalysed biotransformation processes.[10–14]

Self-assembly of surfactants and particles in DES is of particular interest due to their ubiquity in industrial formulations and applications. Raghuwanshi *et al.* investigated self-assembly of gold nanoparticles in reline (a DES comprising choline chloride and urea in a 1 : 2 molar ratio) for green energy applications.[15–18] Hammons *et al.* probed the aggregation of silica particles in reline and ethaline (1 : 2 choline chloride:ethylene glycol).[19–21] The self-assembly behaviour of amphiphiles in various DES has also been studied. Bryant *et al.* reported that phospholipids (1,2-dipalmitoyl-*sn*-glycero-3-phosphocholine, DPPC; 1,2-distearoyl-*sn*-glycero-3-phosphocholine, DSPC; 1,2-dimyristoyl-*sn*-glycero-3-phosphocholine, DMPC; and egg-PC – 16-22 carbon tails with phosphocholine headgroups) formed lamellar (L_α) phases and vesicles[22] in reline, similar to aqueous systems.

Surfactant self-assembly has also been investigated in both reline and glyceline (comprising choline chloride and glycerol in a 1 : 2 molar ratio).[23–25] It has been found that the interfacial self-assembly behaviour of surfactants in the DES is similar to that in aqueous systems. Using surface tensiometry, Sanchez-Fernandez *et al.* reported that cationic surfactants dodecyl/tetradecyl/hexadecyltrimethyl ammonium bromide (C_{12}/C_{14}/C_{16}TAB) displayed a critical micelle concentration (CMC) in glyceline of 22.0, 3.9, and 0.9 mM, respectively.[26] Anionic sodium dodecyl sulfate (SDS) was shown to have a CMC of 2.0 mM in reline[27] and 3.9 mM in glyceline.[28] X-Ray reflectivity (XRR)

[a] *School of Chemistry, University of Bristol, Cantock's Close, Bristol, BS8 1TS, UK. E-mail: wuge.briscoe@bristol.ac.uk*
[b] *Bristol Centre for Functional Nanomaterials, HH Wills Physics Laboratory, University of Bristol, Tyndall Avenue, Bristol BS8 1TL, UK*
[c] *ISIS Muon and Neutron Source, Rutherford Appleton Laboratory, Harwell Oxford, Didcot, OX11 0QX, UK*
[d] *GlaxoSmithKline, St George's Avenue, Weybridge, KT13 0DE, UK*
† Electronic supplementary information (ESI) available. See DOI: 10.1039/d1cp01370j
‡ Current address: ESRF, The European Synchrotron, Grenoble 38043, France.

showed surfactant monolayer formation at the air–reline interface similar to that the air–water interface.[27,28]

However, surfactant self-assembly in the bulk DES solution has shown different behaviours compared to in water or in the individual solvents constituting the DES. For instance, Ruiz-Olles *et al.* observed that 1,3:2,4-dibenzylidene-D-sorbitol (DBS) formed a 'eutectogel' in a range of DES comprising a binary mixture of choline chloride with glycerol, xylitol, sorbitol, or urea.[29] For DBS in reline, SEM and TEM revealed nanofibrillar structures forming an entangled network with a dominant elastic modulus (G'), characteristic of a gel, with a gelation concentration, c = 4 w/v% at 82 °C.

Here, we report gelation of SDS in glyceline at room temperature (RT ~ 25 °C) at low surfactant concentrations, *i.e.* c_{SDS} ~ 1.9 wt%. Surprisingly, the gel phase comprised complex interpenetrating networks of dendritic fractal aggregates of size some hundreds of μm – thus termed a "fracto-eutectogel". For comparison, SDS forms globular micelles in water under the same condition, whilst SDS lamellar gels in glycerol (a glyceline constituent hydrogen-bonding rich solvent) have been reported recently.[30] The microscopic structure of this fracto-eutectogel was visualised with polarising light microscopy (PLM) and its nanostructure studied with small-angle neutron scattering (SANS). Rheology measurements provided complementary information on the gel mechanical properties. The unprecedented observation of the microscopic fractal structures as a result of SDS self-organisation in glyceline points to different molecular interactions in DES compared to aqueous systems or single-component hydrogen-bonding rich solvents.

2. Materials and methods

2.1 Materials

Protonated sodium dodecyl sulfate (h-SDS) (Sigma-Aldrich, >98.0%) was recrystallised three times from ethanol, and its purity was checked with ^{1}H NMR. h-Glycerol (Fisher Scientific, >98.0%) and d-glycerol (Sigma–Aldrich, >98.0% and >98.0 atom%D) were used as received. h-Choline chloride (Sigma–Aldrich, >98.0%) and d_9-trimethyl-choline chloride (Sigma-Aldrich, >98.0% and >98.0 atom%D) were used as received. h-/d-glyceline was prepared by mixing h-/d-choline chloride and h-/d-glycerol in a 1 : 2 molar ratio in a shaker incubator (Stuart SI505) at 550 rpm at 60 °C for two hours (2 h). The gel-like phase was prepared by adding a designated amount of h-SDS to h- or d-glyceline, then incubating the mixture in the shaker incubator at 550 rpm at 60 °C for 2 h before equilibrating at room temperature overnight. All the samples were kept sealed from moisture before measurements, due to hygroscopicity of both choline chloride and glycerol. In a further study, we have examined the effect of water addition systematically (manuscript in preparation).

2.2 Surface tensiometry

Equilibrium surface tension measurements were carried out in ambient conditions with the Wilhelmy plate method using a Krüss K100 tensiometer, with the platinum plate cleaned by flaming between measurements. Due to the relatively high viscosity of h-glyceline (~380 cP), the samples were left to equilibrate for 30 minutes to allow for diffusion of surfactants to the air–liquid interface.

2.3 Viscometry and oscillation rheology

All rheological measurements were performed using a rotational rheometer (Malvern Panalytical Kinexus Pro) in a cone-plate geometry (CP 4/20) to minimise the wall-depletion effect observed in oscillation measurements.[31] Viscometry measurements were carried out with the shear rate, $\dot{\gamma}$, decreasing from 100 s^{-1} to 0.001 s^{-1} and each measurement was run for 3 minutes or until it reached a steady state equilibrium. Oscillation rheology measurements involved first characterising the linear viscoelastic region while changing the deformation, γ, (or the strain rate) applied, at a constant frequency ω = 1 Hz. A strain value was then selected from this linear region, typically γ = 0.012%, for frequency sweep measurements.

2.4 Polarised light microscopy (PLM)

PLM was carried out using an Olympus BX53-P microscope, where the polarisers were crossed at 90° with respect to each other and images were captured using Stream software. PLM measurements were carried out under ambient conditions, using 10, 20, and 40× magnifications. A 530 nm first order waveplate was placed in the optical patch to improve the contrast in some cases.

2.5 Small-angle neutron scattering (SANS)

SANS measurements were made using quartz cells with a 2 mm path length with a 0.5 h integration time on the Loq[32] small-angle diffractometer at the ISIS Pulsed Neutron Source (STFC Rutherford Appleton Laboratory, Didcot, UK). Loq utilizes neutrons with wavelengths λ = 2–10 Å and the data were collected in the q range of 0.008–1.6 $Å^{-1}$, corrected for the detector efficiency, sample transmission, and background scattering and converted to scattering cross-section data ($\partial\Sigma/\partial\Omega$ *vs.* q) using MantidPlot.[33] The data were then converted to an absolute scale (cm^{-1}) using the scattering intensity from a standard sample (a solid blend of hydrogenous and perdeuterated polystyrene).[34]

2.6 SANS data analysis

The SANS data at 25 °C were fitted using two different models. The first was a lamellar paracrystal stack model (Fig. 8b), in which individual SDS lamellae stacks in solution were treated as being independent of each other, with the lamellae considered as a whole rather than separate headgroup and tail layers. The general scattering intensity for the lamellar systems is described as[35–38]

$$I(q) = \frac{2\pi V P(q) S(q)}{\mathrm{d}q^2} \quad (1)$$

where V is the scattering volume, $P(q)$ the form factor that describes the shape of the particles or the phase present, $S(q)$ the structure factor that describes the interparticle interaction, and d the lamellar spacing.

The second model used to fit data at 25 °C was a mass fractal model (Fig. 8c) describing the scattering from fractal-like aggregates in solution[39]

$$I(q) \sim P(q)S(q) \quad (2)$$

where the form factor is

$$P(q) = F(qr)^2 \quad (3)$$

where $r = D/2$ is the radius of the building block or particle. The structure factor is

$$S(q) = \frac{\Gamma(D_m - 1)\xi^{D_m - 1}}{\left[1 + (q\xi)^2\right]^{\frac{(D_m-1)}{2}}} \frac{\sin\left[(D_m - 1)\tan^{-1}(q\xi)\right]}{q} \quad (4)$$

where is the gamma function, ξ the correlation length, and D_m the mass fractal dimension.

3. Results and discussion

3.1 Surface tensiometry measurements of SDS in glyceline

The surface tension, γ, *vs.* $\ln(c_{SDS})$ plots in water, glycerol, and glyceline at room temperature (RT ~ 25 °C) are shown in Fig. 1, with the data for glycerol from ref. 30 included for comparison. The critical micelle concentration, CMC, pure solvent surface tension, γ_0, minimum surface tension, γ_{min}, and the headgroup area, A_{HG}, at ~CMC determined from the surface excess are summarised in Table 1. All three curves show SDS adsorption at the air–liquid interface and an apparent CMC at RT, indicative of SDS surface activity and self-assembly in these solvents.

The cohesive energy and the related Gordon parameter, $G = \gamma_0/V_m^{1/3}$ where V_m is the molecular volume, of a solvent has previously been used to gauge the solvophobic effect in driving self-assembly,[40,41] with a higher G value indicative of a more pronounced solvophobic effect and hence promoting amphiphile self-assembly more strongly.[40,42] Glyceline has a lowest surface tension value compared to water and glycerol (Table 1). This would point to the lowest cohesive energy density of glyceline among the three solvents, as measured by the Gordon parameter.[40,42] The calculated G values for the three solvents are listed in Table 2. However, the CMC of SDS in glyceline is the lowest of the three solvents at 5.4 mM (*vs.* 8.1 and 11.7 mM in water and glycerol, respectively), also with the lowest γ_{min} (Table 1).

The Hildebrand solubility parameter, $\delta_H \sim (CED)^{1/2}$ where CED is the cohesive energy density, is another measure of cohesion. The δ_H values for the three solvents are compared in Table 2, and it shows a different trend to G and cannot be reconciled with the observed CMC (Table 1). This suggests that the self-assembly behaviour of SDS in DES glyceline cannot be readily predicted by the Gordon parameter or the Hildebrand solubility parameter, which have been widely used to gauge the cohesive energy and the solvophobic effect in pure solvents.

Table 1 A summary of the parameters determined from surface tensiometry measurements of SDS in water, glycerol, and glyceline: the surface tension of the pure solvent (γ_0), the minimum surface tension after addition of SDS (γ_{min}), the critical micelle concentration (CMC), the surface excess (Γ), and the surfactant headgroup area (A_{HG}). The data corresponding to SDS at the air–glycerol interface are taken from Ref. 30

Solvent	γ_0 (mN m^{-1})	γ_{min} (mN m^{-1})	CMC (mM)	Γ (10^{-6} mol m^{-2})	A_{HG} (Å^2)
Water	72.8 ± 0.1	38.3 ± 0.1	8.1 ± 0.1	3.82 ± 0.25	43.5 ± 0.9
Glycerol	64.0 ± 0.1	46.0 ± 0.1	11.7 ± 0.1	1.66 ± 0.38	46.0 ± 0.5
Glyceline	63.5 ± 0.1	34.2 ± 0.1	5.4 ± 0.2	4.29 ± 0.59	38.7 ± 0.3

Table 2 Cohesion dependent parameters taken from the literature of water, glycerol, and glyceline: Hildebrand solubility parameter (δ_H) and the Gordon parameter (G)

Solvent	δ_H (MPa$^{1/2}$)	CED (MPa)	G (J m^{-3})
Water	34.2[41]	1169.6	2.75[40]
Glycerol	29.2[41]	852.6	1.51[40]
Glyceline	31.0[42,a]	961.0	1.20[42,a]

[a] Denotes that the molecular volume used in the calculation was determined from simulations.

3.2 The formation of a gel in glyceline

Fig. 2 shows a series of glyceline samples in inverted glass vials containing SDS at different concentrations, c_{SDS} = 0.1–5.3 wt%

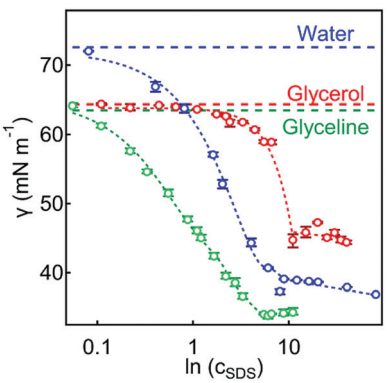

Fig. 1 Surface tension, γ, *vs.* $\ln(c_{SDS})$ for SDS at the air–water (red circles), air–glycerol (blue circles), and air–glyceline (green circles) interfaces at room temperature (RT). The surface tensions of the pure solvents, γ_0, are indicated by the horizontal dashed lines. The curve corresponding to SDS at the air–glycerol interface is taken from ref. 30.

Fig. 2 (a) Inverted vials containing ~2 mL of transparent SDS solution in glyceline with c_{SDS} = 0.1–5.3 wt% (labels in b, concentrations are in wt%) immediately after they were heated at 60 °C and shaken at 550 rpm for 2 h. (b) After being left overnight at room temperature (RT ~ 25 °C), the samples with $c_{SDS} \geq 1.9$ wt% (~12.6 CMC) SDS formed an opaque gel-like phase (*i.e.* samples 5–12 with c_{SDS} = 1.9–5.3 wt%).

Table 3 SDS concentrations (in wt%) for the samples in Fig. 2, and the sample numbers are applicable to both Fig. 2a and b

Sample no.	1	2	3	4	5	6	7	8	9	10	11	12
c_{SDS} (wt%)	0.1	0.3	0.6	1.2	1.9	2.5	2.9	3.4	3.9	4.4	4.8	5.3

(*i.e.* 5–220 mM; 0.9–37.0 CMC; *cf.* Table 3). At 60 °C, all the samples were transparent and fluid (Fig. 2a); however, when cooled to RT ~ 25 °C, an opaque phase formed. At $c_{SDS} \geq 1.9$ wt%, the sample could hold its weight upon inversion (Fig. 2b). In contrast, SDS in aqueous solutions formed transparent fluid phases consistent with globular micellar solutions.[43–45] For comparison, opaque SDS gel phases have been observed in glycerol,[30] with a critical gelation SDS concentration of $c_{CGC} \sim 2$ wt% (or 110 mM) below a critical gelation temperature of $T_{GC} \sim 45$ °C.[30] The observation of SDS gelation in glyceline suggests interpenetrated networks of aggregates at RT, which would break up at elevated temperatures. Such an SDS-in-glyceline gel (or in other DES), at low SDS concentrations, has not been previously reported in the literature to our knowledge.

3.3 Rheological properties of the fracto-eutectogel

A representative plot of shear stress, σ, as a function of shear rate, $\dot{\gamma}$, of the SDS-in-glyceline gel (5.3 wt%, ~53 CMC) is shown in Fig. 3a, displaying shear thinning behaviour with a non-linear stress-rate (σ–$\dot{\gamma}$) relationship. The magnitude of σ (<100 Pa) is consistent with a weak physical gel that can be disturbed by the applied shear, indicated by the presence of an inflection point at $\dot{\gamma} \sim 5$ s^{-1} in the σ–$\dot{\gamma}$ plot. This behaviour is similar to previously reported gel phases consisting of fibrillar aggregates.[46–51] Fig. 3b shows the variation of the shear viscosity, η, with c_{SDS} at two different shear rates (taken from linear fits before and after the inflection point). At the lower shear rate (0–5 s^{-1}; LSR), η_{LSR} increased linearly with c_{SDS}, in contrast to the constant η_{HSR} at the higher shear rate (5–100 s^{-1};HSR). This suggests that the 3D structure in the gel phase was broken up at the HSR into smaller aggregates, manifesting in a constant viscosity value over the c_{SDS} range.

The behaviour of the first normal stress difference, N_1, (Fig. 3a, inset) is different from that expected of fibrillar dispersions, for which N_1 would typically increase with $\dot{\gamma}$ due to fibrous aggregates becoming elongated in the direction of the applied shear.[52–54] Here, N_1 decreased with $\dot{\gamma}$ (for $\dot{\gamma} > \sim 0.05$ s^{-1}), indicating that the aggregates became shorter in the direction of the applied shear. The decreasing N_1 with $\dot{\gamma}$ can be attributed to hydrodynamic friction between individual aggregates,[55,56] implying the presence of globular aggregates. Unlike the shear thickening behaviour often observed in colloidal dispersions due to shear-induced aggregation,[57,58] the shear thinning and N_1 behaviour observed in this study suggest that, while the aggregates showed hydrodynamic friction, there was no flocculation-induced shear thickening, a behaviour observed in some colloidal gels.[59,60]

The elastic and viscous moduli (G' and G'', respectively) are shown as a function of the deformation (or strain, γ, Fig. 4a) to demonstrate the viscoelastic behaviour of the 5.3 wt% SDS-in-glyceline gel in response to an applied deformation. The presence of a linear viscoelastic region (LVER) at small deformations ($\gamma \sim 0.001$–0.1%) shows that the structure of the gel was unaffected by small strains.

A previous report showed that the magnitude of $G'(\gamma)$ and $G''(\gamma)$ of an SDS-in-glycerol gel was an order of magnitude higher than that observed here.[30] The MacKintosh model, assuming the system consisting of a semiflexible network,[61] relates the bending modulus, κ, of the constituent fibres to the gel elastic modulus, $G'_{LVER}(\gamma) \sim \kappa^2$. The estimated κ values using this model are plotted against c_{SDS} in Fig. 5, showing a

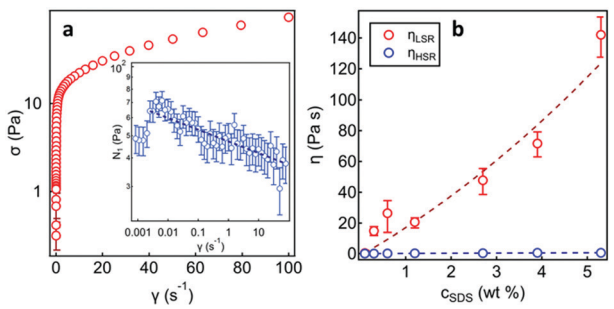

Fig. 3 (a) Shear stress, σ, *vs.* shear rate $\dot{\gamma}$, for the SDS-in-glyceline gel (5.3 wt %, ~53 CMC); inset: corresponding first normal stress difference, N_1, *vs.* shear rate, $\dot{\gamma}$. (b) Shear viscosity, η, *vs.* SDS concentration, c_{SDS}, for the SDS-in-glyceline gel, where η was obtained by taking the gradient in the appropriate regime of the σ–$\dot{\gamma}$ plot (red circles – low shear rate, LSR; blue circles – high shear rate, HSR).

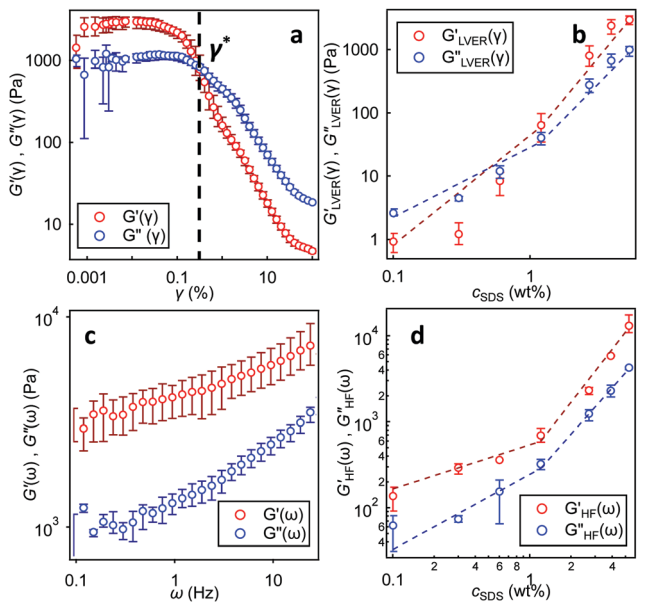

Fig. 4 (a) G' (elastic, red) and G'' (viscous, blue) as a function of shear strain, γ, at a frequency ω = 1 Hz for the gel (5.3 wt% SDS), showing the initial plateau linear viscoelastic region (LVER). (b) Variation of G' and G'' with c_{SDS}, with the modulus values taken from the plateau regions ($\gamma < 0.2\%$) in (a). c_{CGC} refers to the critical gelation concentration. (c) G' and G'' as a function of shear frequency, ω, for the gel (5.3 wt% SDS) at the strain rate γ = 0.012%. (d) Variation of G' (elastic, red) and G'' (viscous, blue) with c_{SDS} at ω = 10 Hz, with the subscript HF denoting the higher frequency range. Dashed lines are guidelines for the eye and do not represent a true fit for the data.

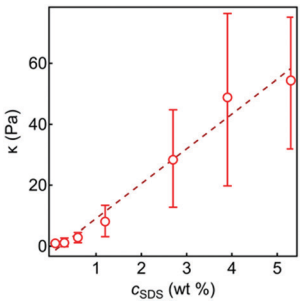

Fig. 5 The bending modulus, κ, as a function of c_{SDS} with a linear guide-line. κ was determined from the MacKintosh model[61] using the plateau G' values from the amplitude sweep measurements. The dashed line is a guide for the eye.

linear relationship, with a maximum κ value of ~50 Pa, which was lower than that observed for the SDS-in-glycerol gel ($\kappa \sim 140$ Pa).

The behaviour of $G'(\gamma)$ and $G''(\gamma)$ beyond the LVER shows the sensitivity of the gel network to the applied deformation, as both moduli decreased by two orders of magnitude, possibly due to the breakup of the larger aggregates into smaller ones. The gel appeared elastic at low deformations ($\gamma < 0.2\%$), with $G'(\gamma) > G''(\gamma)$; however, a crossover point is observed at $\gamma^* \sim 0.3\%$, above which $G''(\gamma) > G'(\gamma)$, indicating a transition to a more liquid-like phase.

The values of the LVER elastic and viscous moduli as a function of c_{SDS} are shown in Fig. 4b. As c_{SDS} increased, a transition from a liquid-like to a solid-like material can be observed at $c_{SDS} \sim 1.2$ wt% (the slopes of the G'/G'' *vs.* c_{SDS} plots before and after the transiton are listed in Table 4). This concentration can be deemed (as similarly defined in ref. 30) a critical gelation concentration, c_{CGC}, consistent with the macroscopic observations in the inverted vial test (Fig. 2).

The gel structure appeared to be more sensitive to the magnitude of deformation than the speed at which it was applied. Fig. 4c shows the variation of G' and G'' at low strain ($\gamma < 0.2\%$) as a function of the shear frequency, ω, for the 5.3 wt% SDS-in-glyceline gel. Over the ω range measured, the elastic modulus remained dominant (*i.e.* $G' > G''$) with no crossover, indicating a solid-like behaviour. Whilst the gel showed sensitivity to strains, γ, the moduli were less sensitive to the frequency, ω. The absence of the $G'(\omega)$–$G''(\omega)$ crossover would suggest that the system was not comprised of fibrillar aggregates[62] – and instead more likely of globular aggregates. The magnitudes of the two moduli ($G' \sim 12.5$ kPa and $G'' \sim 4$ kPa) are quite high compared to surfactant-based gels of elongated wormlike micelles[63–66] (in the range of 10–100 Pa). However, these values are comparable to those of the SDS-in-glycerol gel ($G' \sim 27$ kPa and $G'' \sim 11$ kPa).[30]

The dependence of G' and G'' (at a high frequency $\omega = 10$ Hz) on c_{SDS} is shown in Fig. 4d, with a similar transition (*cf.* Table 4) observed compared to the amplitude sweep data (Fig. 4b). Whilst the $G'(\omega)$ and $G''(\omega)$ magnitude increased with c_{SDS}, there was no crossover and the elastic modulus remained dominant ($G'(\omega) > G''(\omega)$) even in the liquid regime. The lack of a crossover arises from the lower sensitivity of globular aggregates to the speed at which the deformation is applied, without structural changes observed in the globular aggregates. This again suggests that the structure of the gel consisted of particulates, akin to a colloidal gel.[67]

Table 4 Values for the slopes in the liquid and gel regimes of the plots of the elastic (G') and viscous (G'') moduli *vs.* c_{SDS} for the amplitude (γ from the LVER) and frequency ($\omega = 10$ Hz) sweep measurements in Fig. 4b and d, respectively

Modulus	Regime/phase	Modulus *vs.* c_{SDS} slope (Pa)
$G'(\gamma)$	Liquid	54.7
	Gel	701.3
$G''(\gamma)$	Liquid	29.8
	Gel	214.8
$G'(\omega)$	Liquid	389.5
	Gel	3122.5
$G''(\omega)$	Liquid	230.6
	Gel	937.0

3.4 Microscopic structure of the ordered surfactant mesophase

Polarised light microscopy (PLM) revealed an anisotropic mesophase at room temperature at SDS concentrations ($c_{SDS} >$ 1.9 wt%) (Fig. 6), consisting of dendritic feather-like aggregates of some μm in length scale with no particular alignment. The dendritic fractal[68,69] morphology (seen in detail in Fig. 6c, d) exhibits a central fibre that supports secondary fibres, which in turn support tertiary fibres, and so on. A fibre order parameter, n_f, can be defined as the fibre position away from the parent or central fibre, where the parent fibre $n_f = 1$. As n_f increases, both the fibre length and the diameter generally decrease (Fig. 7b). It is conceivable that the fibres grew sequentially: first the growth of the parent fibres, then the secondary fibres and the tertiary fibres. The detailed mechanism – whether the parent and child

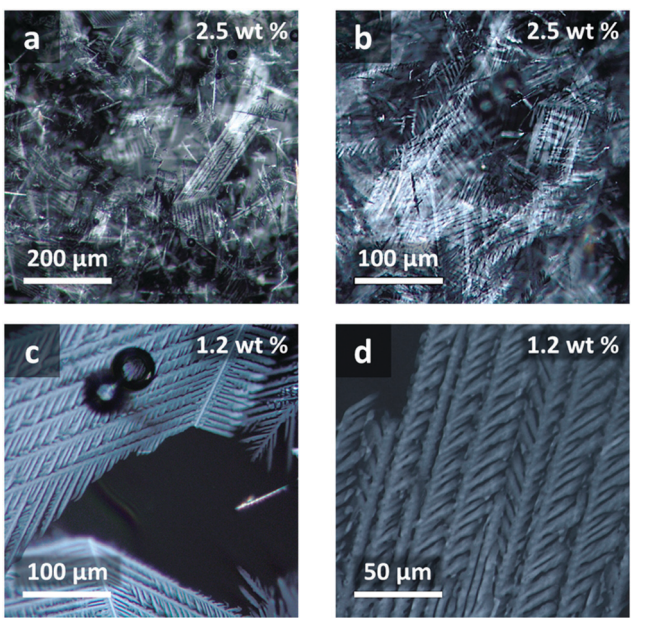

Fig. 6 PLM images of the dendritic feather-like aggregates present in SDS in glyceline at RT at magnifications of 10× (a), 20× (b and c), and 40× (d), with the c_{SDS} indicated.

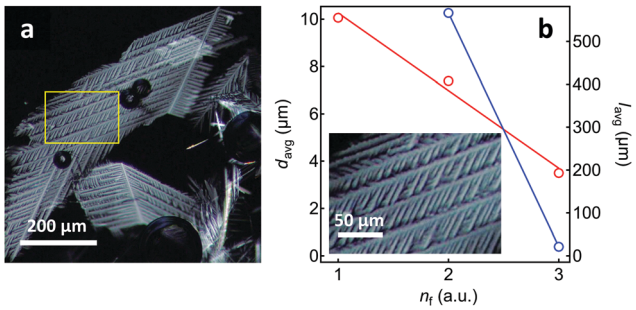

Fig. 7 (a) PLM image of the feather-like aggregates in 1.2 wt% SDS-in-glyceline gel, with the rectangular region showing where tertiary fibres were measured. (b) Average lengths, l_{avg} (blue circles), and diameters, d_{avg} (red circles), of fibres *vs.* the fibre order, n_f. (inset) The highlighted region in (a) magnified for clarity.

fibres grow simultaneously, or the parent grows first and then stops to allow the children to grow – is unclear.

3.5 Gel nanostructure from SANS

Fig. 8 shows the SANS scattering profiles at different c_{SDS}, with the data fitted to a mass fractal model (Fig. 8c) and, for c_{SDS} = 1.2, 2.7, and 5.3 wt%, also a lamellar paracrystal model (Fig. 8b).

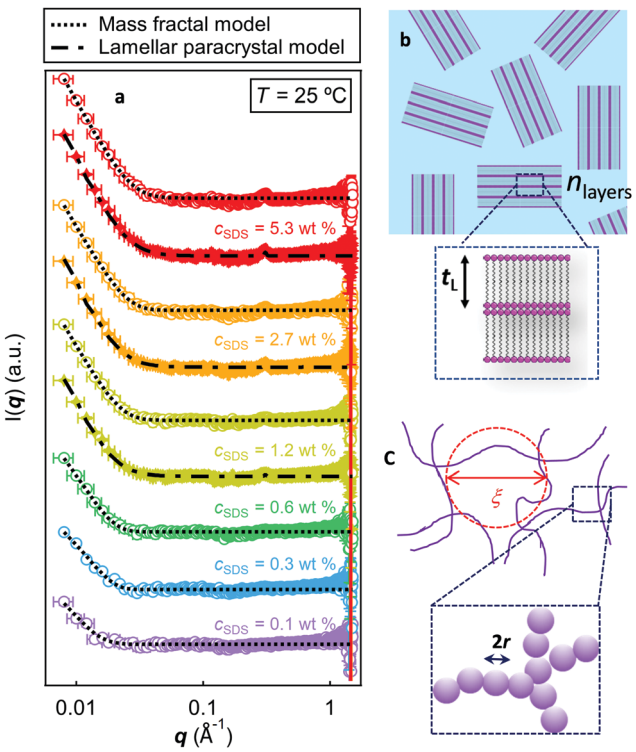

Fig. 8 (a) SANS profiles for h-SDS in *d*-glyceline at varying surfactant concentrations, c_{SDS}, at T = 298 K. At c_{SDS} = 0.1, 0.3. and 0.6 wt%, the SANS curves were fitted with a mass fractal model (dotted lines); whilst at c_{SDS} = 1.2, 2.7. and 5.3 wt%, the data was also fitted with the lamellar paracrystal model (dot-dashed lines), capturing well the single bragg peak. The SANS profiles are offset on the vertical scale for clarity. Schematic representations of: (b) the lamellar stack paracrystal model, with randomly oriented lamellar domains consisting of nlayers of bilayers of thickness tL; and (c) the mass fractal model, where $2r = D$ is the building block diameter and ξ the correlation length.

The appearance of a Bragg peak at $q \sim 0.30$ Å^{-1} at the higher SDS concentrations (c_{SDS} = 1.2, 2.7 and 5.3 wt%), corresponding to $d \sim 2\pi/q \sim 20.9$ Å, suggests the formation of an ordered mesophase. There was no plateau observed in the low-q region of the SANS scattering profiles at any c_{SDS}, indicating the presence of a large structure or mesophase in the gel whose size was not accessible in the q-range of the SANS measurement.

The coherence length, L_c, which is indicative of the disorder of the meso-structure, can be obtained from analysing the broadening of the Bragg peaks using the Scherrer equation[70–76]

$$L_c = \frac{2\pi K}{\Delta q} \quad (5)$$

where K is a shape factor (here $K \sim 1$), and Δq is the full width at half maximum of the Bragg peak.

The L_c *vs.* c_{SDS} behaviour (Fig. 9) appears different at low c_{SDS} (1.2 wt%) compared to the two higher c_{SDS} samples (2.7 and 5.3 wt%), implying different structural orders. The L_c value at the two higher c_{SDS} converged to $L_c \sim 140$ Å at T = 40 °C.

As only one Bragg peak is present in the scattering profile, it cannot ascertain the exact mesophase type; this peak could also arise from the presence of solid SDS crystallites. Complementary X-ray reflectivity (XRR) measurements at the air-glyceline interface (Fig. S1, ESI†) showed the presence of a second Bragg peak at $q \sim 0.6$ Å^{-1}, consistent with the n_α = 1, 2 peaks of a lamellar phase or surfactant crystal. A recent study has similarly shown the presence of aggregates with a lamellar structure in SDS-in-glycerol gel,[30] and thus the obtained SANS profile was fitted to a lamellar paracrystal stack model (Fig. 8b). The fits to 5.3, 2.7, and 1.2 wt% h-SDS in d-glyceline are shown in Fig. 8 with the fitting parameter values in Table 5. The reduced intensity and number of Bragg peaks observed in this study – as compared in glycerol in the previous study[30] – could be attributed to the presence of choline chloride in glyceline, which could disrupt the structural order of the SDS lamellar phase.

The thickness, t_L, and the d-spacing of the lamellar phase show a close agreement, $t_L \sim d \sim 20$ Å (*cf.* Fig. 8b), indicating

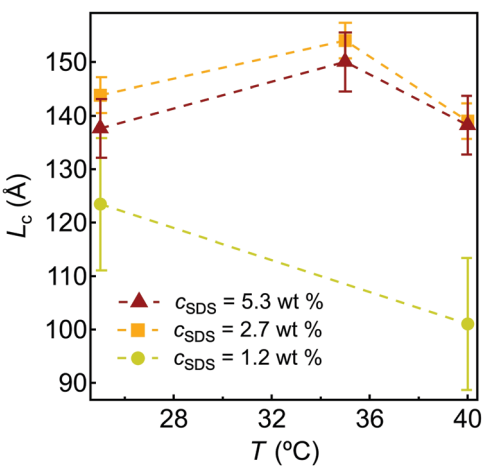

Fig. 9 The coherence length, L_c, calculated using the Scherrer equation, with the full-width half maximum (FWHM) determined through a Gaussian peak analysis.

Table 5 Fitting parameters for the paracrystalline lamellar stack model for c_{SDS} = 1.2, 2.7 and 5.3 wt% h-SDS in *d*-glyceline at RT ~ 25 °C (*cf.* Fig. 1a): SDS bilayer thickness t_L, number of layers in the stack n_{Layers}, *d*-spacing, polydispersity of the *d*-spacing σ_d, scattering length density of SDS ρ_{SDS}, scattering length density of glyceline ρ_{Gly}, polydispersity of the SDS bilayer thickness σ_t, and chi squared value χ^2(as a measure of the goodness of the fit)

Lamellar paracrystal stack parameters	c_{SDS} (wt%)		
	1.2	2.7	5.3
t_L (Å)	20.0	20.0	20.0
n_{Layers}	57.7	57.7	57.7
d-Spacing (Å)	20.4	20.4	20.4
σ_d (Å)	0.012	0.012	0.013
ρ_{SDS} (10^{-6} Å^{-2})	0.43	0.43	0.40
ρ_{Gly} (10^{-6} Å^{-2})	5.85	5.84	5.50
σ_t	1.0	1.0	1.0
χ^2	4.4	3.8	3.8

that the lamellar sheets consisted solely of SDS bilayers. A full SDS bilayer of thickness of two SDS lengths would give t_L ~ 35–45 Å; however, smaller SDS lamellar spacing has been reported, t_L ~ 25–28 Å[77,78] in the presence of additives, such as a co-solvent. The smaller value reported here, t_L ~ 20 Å, could arise from a tilted SDS bilayer or interpenetration of the tails. The high polydispersity of the lamellar thickness implies polymorphisms with different SDS packing and conformations, leading to different *d*-spacing. We acknowledge that, along with the large thickness polydispersity, the presence of a single Bragg peak and the relatively small fitted t_L value could mean the paracrystal lamellar model might not best describe data.

Fractal models were also trialled to fit the SANS data – to capture the structural features at larger length scales. Of these, the mass fractal model[39] was found to best fit the SANS profiles at 25 °C (Fig. 8a, c and Table 6). The fitted radii, *r*, of the aggregates decreased with increasing c_{SDS}, a feature also evident from PLM (Fig. S2, ESI†), where larger aggregates were more noticeable at lower c_{SDS}. This could be due to the growth of the aggregates being stunted by the number of aggregates forming, suggesting that the growth mechanism is that all fibre orders (n_f = 1, 2, and 3) grow simultaneously.[79]

The fractal dimension, D_m, is related to the Hausdorff dimension,[80,81] which is a mathematical description of scale invariances that appear identical when viewed over a range of scales. Mass fractals typically have D_m ~ 2–3; for instance broccoli has a D_m ~ 1.8 and cauliflower a D_m ~ 1.9.[82] D_m ~ 2 is indicative of smoother aggregates and D_m ~ 3 is from rougher aggregates,

Table 6 Fitting parameters for the mass fractal model used to simulate the data for h-SDS in *d*-glyceline at different SDS concentrations (c_{SDS}) at 25 °C (*cf.* Fig. 1b): building block radius *r*, fractal dimension D_m, and chi squared value χ^2

c_{SDS} (wt%)	*r* (Å)	D_m	χ^2
0.1	20.0	3.37	4.9
0.3	145.6	2.30	6.9
0.6	128.5	2.65	4.5
1.2	88.5	2.97	4.4
2.7	77.5	2.91	3.0
5.3	56.5	2.95	3.4

Table 7 Fractal dimensions, D_m, of SDS in glyceline at different c_{SDS}, estimated through a power-law fit to the low-***q*** region of the SANS profiles at different SDS concentrations

c_{SDS} (wt%)	D_m
0.1	2.6 ± 0.7
0.3	2.8 ± 0.6
0.6	2.6 ± 0.2
1.2	1.9 ± 0.1
2.7	1.5 ± 0.1
5.3	1.5 ± 0.2

with $D_m > 2$ implying three dimensional fractals.[83,84] Table 5 shows D_m ~ 2.8–3 across the c_{SDS} studied, indicating very rough mass fractal aggregates of similar D_m to that reported of human lungs.[85]

The fractal dimension can also be estimated directly from a power law fit to the low-***q*** data of the scattering profile,[39] *i.e.* ~ q^{D-6} (Table 7). This yielded lower D_m values (1.5–2.8) compared to those obtained through the fitting to the SANS profiles of the higher c_{SDS}. This difference could be due to the sensitivity of the mass fractal model regarding the dimensionality of the interfacial region between the cluster and solvent bulk, as opposed to the cluster itself, as noted by Mildner and Hall.39

4. Summary, further discussions and proposed gelation mechanism

We have observed the formation of a gel in glyceline, a deep eutectic solvent (DES), at an SDS critical gelation concentration as low as c_{CGC} ~ 1.9 wt% (*i.e.* 12.7 CMC). PLM revealed that the gel phase comprised fractal dendritic aggregates of ~mm in size, consistent with the SANS data fitted using a mass fractal model. At comparable c_{SDS}, SDS would form spherical micellar aggregates in water as expected from its packing parameter of ~ 0.25.[86,87] At much higher concentrations and at higher *T* (> 80 °C), SDS would form lamellar or hexagonal phases (c_{SDS} ~ 75 and 45 wt%, respectively).[43,44] The formation of dendritic fractal aggregates has not been reported, and we term it a fracto-eutectogel.

The dendritic aggregates oriented anisotropically and their hierarchical structures might be considered as comprising parent and child fibres. The fibre length and diameters of the fibres decreased with increasing fibre order, n_f, implying that the growth of the parent fibre preceded the child fibres. Rheology measurements confirmed relatively weak interactions of the network entanglement, akin to a physical colloidal gel. The negative first normal stress difference, N_1, and elastic properties of the gel phase were consistent with a colloidal gel comprising globular aggregates in solution.

Dendrites are fern-like or tree-like fractals common in nature, such as hoarfrost,[88] and have been widely studied. The driving force for dendrite formation is related to the Mullins–Sekerka instability.[89–92] It describes the progression of a solid front, or the dendrite tip, in a liquid medium, where the cooled solid advances into a warm, or undercooled, medium.[93,94] For growth to occur, the interface must be warmed to the

temperature of the liquid, typically as a result of latent heat released by kinks along an otherwise smooth surface.[95,96] The growth of fractals, and dendritic patterns in particular, is driven by surface tension anisotropy as proposed by Gruber and Mullins,[97] where the surface tension of perturbed surfaces deviates from that of unperturbed planar surfaces.[98,99]

SANS measurements showed the formation of a bulk mesophase at all c_{SDS} studied, well described by a mass fractal model with a fractal dimension D_m = 2.8–3.0 in the gel phase (or a smaller value using the power law fit to the low q SANS data), confirming the PLM visualization. This contrasts with SDS self-assembly in aqueous systems,[43,44,78] forming globular aggregates at comparable c_{SDS}.

The morphological details of the fracto-eutectogel are also quite unusual for non-aqueous systems. For example, an SDS-in-glycerol gel[30] has been recently reported at comparable c_{SDS} at RT, comprising fibrous networks of lamellar building blocks. Here, a lamellar model could well capture the Bragg peaks in the SANS data (Fig. 8), suggesting lamellar packing of SDS in the dendritic fractal aggregates as observed in hydrated crystalline systems.[100] Surfactants are known to form hydrated crystals below the Krafft point[101] and crystallisation of inorganic ions in DES has also been reported.[102,103] Gelation and crystallisation are often viewed as two competing processes.[104,105] However, the crystal engineering approach to forming supramolecular gels has been reported.[106,107] For instance, anthracenyl groups of cholesteryl 4-(2-anthryloxy)butanoate (CAB) forms a stacked helical arrangement, leading to a thermally reversible gel network;[107,108] inulin gels comprise networks of small crystallites.[109]

The contrast between the observation in glyceline (choline chloride : glycerol in 1 : 2 ratio) here and in glycerol[30] points to the pivotal role of choline chloride in facilitating the formation of fractal aggregates. We note that a critical gelation temperature, T_{GC}, exists, above which SDS forms cylindrical aggregates.

The role of choline chloride in the self-assembly of such aggregates may be explained by the counterion condensation theory,[110] commonly used to describe polyelectrolyte systems but also extended to other systems.[111–113] In our system, the parent fibre grows in one dimension into a rod-like shape and simultaneously choline ions are diffusing to the fibre surface through counterion condensation (Fig. 10). The condensed choline ions lead to certain points along the fibre that radiate heat more effectively, causing kinking along the otherwise flat rod surface as a result of Mullins–Sekerka instability.[89–92] Due to the bridging effect of the condensed choline ions, this leads to increased growth at the kink sites, resulting in branching and dendritic growth[95,96] (Fig. 10f). Such a counterion condensation effect is more favourable in glyceline due to its lower dielectric constant ($\varepsilon_{Glyceline} \sim 10\,114$ *vs.* 78.3[115] and 42.5[116] for water and glycerol, respectively), due to stronger attractions between opposite ions and, in turn, a stronger bridging effect. Such cation-bridging has been observed;[117–119] for instance, SDS and caesium dodecyl sulfate formed hemicylinders bridged with Na^+/Cs^+ counterions at the water-graphite interface.[119]

At $c_{SDS} > 1.9$ wt%, jamming of the fractal aggregates – rather than their interpenetration – would lead to a colloidal gel, consistent with the rheological observations, which indicate a structure closer to a colloidal gel rather than an entangled fibrillar network.

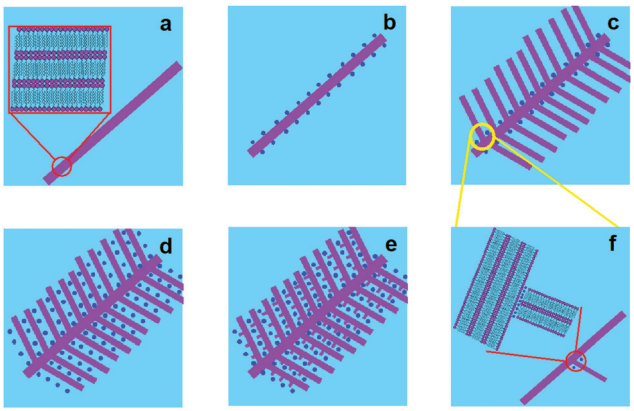

Fig. 10 Schematic representation of the growth mechanism for the dendritic fractal aggregates: (a) a parent fibre comprising a tightly packed SDS crystals. (b) Diffusion-limited counterion condensation along the parent fibre, leading to dendritic growth (c). (d) Diffusion limited counterion condensation along the dendrites, leading to further dendritic growth (e). (f) A magnified cartoon of the contact between parent and child fibres.

Fractal aggregates exist already at low SDS concentration ($c_{SDS} \sim 0.1$ wt%) evident from PLM observations (Fig. S3 in ESI†) with the constituent fibres appearing thicker possibly due to a smaller number of nucleation sites at the lower SDS concentration.

The SDS Krafft point in glycerol, a component of glyceline, is $T_k > 30$ °C,[120] below which crystallisation of surfactants is favoured over self-assembly.[121] Surface tensiometry measurements (Fig. 1) however points to SDS surface activity and thus self-assembly tendency at RT. Addition of salt has been shown to alter the Krafft point of ionic surfactants,[122–124] and the presence of choline chloride could thus suppress the Krafft point, giving rise to the self-assembly tendency of SDS observed at RT.

Further experimental work would be required to fully validate the proposed formation mechanism for the fracto-eutectogel of SDS in glyceline. For instance, use of cationic, zwitterionic, and a nonionic surfactants (*e.g.* DTAB, cocobetaine, and C_5E_{12} respectively) would inform whether the cationic choline ion would stabilise the different types of headgroup. Our results have fundamental implications to gelation and self-assembly important in application of DES as green solvents.

Author contributions

Lauren Matthews: data curation, formal analysis, methodology, investigation, validation, visualisation, writing – original draft. Silvia Ruscigno: data curation, investigation. Sarah E. Rogers: resources, methodology, investigation. Paul Bartlett: funding acquisition, conceptualisation, supervision. Andrew J. Johnson: resources, project administration, supervision. Robert Sochon: funding acquisition, conceptualisation, resources, project administration, supervision. Wuge H. Briscoe: funding acquisition, conceptualisation, resources, methodology, formal analysis,

validation, supervision, project administration, writing – reviewing and editing.

Conflicts of interest

The authors declare no conflict of interest.

Acknowledgements

We acknowledge the ISIS Muon and Neutron Source for the awarded beamtime under experiment number: RB1810629, and the Diamond Light Source for the awarded beamtime under experiment number SI20171-2. We thank A. Seddon (Bristol Physics) for use of the polarising light microscope (PLM). We thank A. Slastanova, J. Rawle, and H. Stockdale for their help with the XRR experiments, and Ż. Przybyłowicz, and S. Michel for their help with the SANS experiments. L.M. was supported by a studentship jointly funded through the Engineering and Physical Science Research Council (the Bristol Centre for Functional Nanomaterials (EPSRC, EP/L016648/1)) and GlaxoSmithKline. SasView, originally developed under NSF award DMR-0520547, contains code developed with funding from the European Union's Horizon 2020 research and innovation programme under the SINE2020 project, grant agreement No 654000.

References

1 A. P. Abbott, G. Capper, D. L. Davies, H. L. Munro, R. K. Rasheed and V. Tambyrajah, Preparation of novel, moisture-stable, Lewis-acidic ionic liquids containing quaternary ammonium salts with functional side chains, *Chem. Commun.*, 2001, 2010.

2 E. L. Smith, A. P. Abbott and K. S. Ryder, Deep Eutectic Solvents (DESs) and Their Applications, *Chem. Rev.*, 2014, **114**(21), 11060.

3 K. R. Seddon, Ionic liquids - A taste of the future, *Nat. Mater.*, 2003, **2**(6), 363.

4 R. D. Rogers and K. R. Seddon, Ionic liquids - Solvents of the future?, *Science*, 2003, **302**(5646), 792.

5 A. P. Abbott, M. Azam, G. Frisch, J. Hartley, K. S. Ryder and S. Saleem, Ligand exchange in ionic systems and its effect on silver nucleation and growth, *Phys. Chem. Chem. Phys.*, 2013, **15**(40), 17314.

6 A. P. Abbott, G. Capper, B. G. Swain and D. A. Wheeler, Electropolishing of stainless steel in an ionic liquid, *Trans. Inst. Met. Finish.*, 2005, **83**(1), 51.

7 A. P. Abbott, K. El Ttaib, G. Frisch, K. J. McKenzie and K. S. Ryder, Electrodeposition of copper composites from deep eutectic solvents based on choline chloride, *Phys. Chem. Chem. Phys.*, 2009, **11**(21), 4269.

8 A. P. Abbott, K. El Ttaib, G. Frisch, K. S. Ryder and D. Weston, The electrodeposition of silver composites using deep eutectic solvents, *Phys. Chem. Chem. Phys.*, 2012, **14**(7), 2443.

9 A. P. Abbott, K. J. McKenzie and K. S. Ryder, Electropolishing and Electroplating of Metals Using Ionic Liquids Based on Choline Chloride, *ACS Symp. Ser.*, 2007, **975**, 186.

10 N. Guajardo, C. R. Muller, R. Schrebler, C. Carlesi and P. D. de Maria, Deep Eutectic Solvents for Organocatalysis, Biotransformations, and Multistep Organocatalyst/Enzyme Combinations, *ChemCatChem*, 2016, **8**(6), 1020.

11 J. T. Gorke, F. Srienc and R. J. Kazlauskas, Hydrolase-catalyzed biotransformations in deep eutectic solvents, *Chem. Commun.*, 2008, 1235.

12 J. Gorke, F. Srienc and R. J. Kazlauskas, ORGN 299-Deep eutectic solvents: Alternative reaction media for hydrolase-catalyzed reactions, *Abstracts of Papers of the American Chemical Society*, 2008, 236.

13 J. Gorke, F. Srienc and R. Kazlauskas, Toward Advanced Ionic Liquids. Polar, Enzyme-friendly Solvents for Biocatalysis, *Biotechnol. Bioprocess Eng.*, 2010, **15**(1), 40.

14 P. D. de Maria and Z. Maugeri, Ionic liquids in biotransformations: from proof-of-concept to emerging deep-eutectic-solvents, *Curr. Opin. Chem. Biol.*, 2011, **15**(2), 220.

15 V. S. Raghuwanshi, M. Ochmann, F. Polzer, A. Hoell and K. Rademann, Self-assembly of gold nanoparticles on deep eutectic solvent (DES) surfaces, *Chem. Commun.*, 2014, **50**(63), 8693.

16 V. Raghuwanshi, M. Ochmann, F. Polzer, A. Hoell and K. Rademann, Growth mechanisms of self-assembled gold nanoparticles in Deep Eutectic Solvent, *Acta Crystallogr., Sect. A: Found. Adv.*, 2014, **70**, C891.

17 V. S. Raghuwanshi, M. Ochmann, A. Hoell, F. Polzer and K. Rademann, Deep Eutectic Solvents for the Self-Assembly of Gold Nanoparticles: A SAXS, UV-Vis, and TEM Investigation, *Langmuir*, 2014, **30**(21), 6038.

18 M. O'Neill, V. S. Raghuwanshi, R. Wendt, M. Wollgarten, A. Hoell and K. Rademann, Gold Nanoparticles in Novel Green Deep Eutectic Solvents: Self-Limited Growth, Self-Assembly & Catalytic Implications, *Z. Phys. Chem.*, 2015, **229**(1-2), 221.

19 J. A. Hammons, F. Zhang and J. Ilaysky, Extended hierarchical solvent perturbations from curved surfaces of mesoporous silica particles in a deep eutectic solvent, *J. Colloid Interface Sci.*, 2018, **520**, 81.

20 J. A. Hammons, J. Ustarroz, T. Muselle, A. A. J. Torriero, H. Terryn, K. Suthar and J. Ilavsky, Supported Silver Nanoparticle and Near-Interface Solution Dynamics in a Deep Eutectic Solvent, *J. Phys. Chem. C*, 2016, **120**(3), 1534.

21 J. A. Hammons, T. Muselle, J. Ustarroz, M. Tzedaki, M. Rats, A. Hubin and H. Terryn, Stability, Assembly, and Particle/Solvent Interactions of Pd Nanoparticles Electrodeposited from a Deep Eutectic Solvent, *J. Phys. Chem. C*, 2013, **117**(27), 14381.

22 S. J. Bryant, R. Atkin and G. G. Warr, Spontaneous vesicle formation in a deep eutectic solvent, *Soft Matter*, 2016, **12**(6), 1645.

23 A. Sanchez-Fernandez, G. L. Moody, L. C. Murfin, T. Arnold, A. J. Jackson, S. M. King, S. E. Lewis and K. J. Edler, Self-assembly and surface behaviour of pure and mixed zwitterionic amphiphiles in a deep eutectic solvent, *Soft Matter*, 2018, **14**(26), 5525.

24 M. Pal, R. K. Singh and S. Pandey, Evidence of Self-Aggregation of Cationic Surfactants in a Choline Chloride

plus Glycerol Deep Eutectic Solvent, *ChemPhysChem*, 2015, **16**(12), 2538.
25 M. Pal, R. Rai, A. Yadav, R. Khanna, G. A. Baker and S. Pandey, Self-Aggregation of Sodium Dodecyl Sulfate within (Choline Chloride plus Urea) Deep Eutectic Solvent, *Langmuir*, 2014, **30**(44), 13191.
26 A. Sanchez-Fernandez, T. Arnold, A. J. Jackson, S. L. Fussell, R. K. Heenan, R. A. Campbell and K. J. Edler, Micellization of alkyltrimethylammonium bromide surfactants in choline chloride: glycerol deep eutectic solvent, *Phys. Chem. Chem. Phys.*, 2016, **18**(48), 33240.
27 T. Arnold, A. J. Jackson, A. Sanchez-Fernandez, D. Magnone, A. E. Terry and K. J. Edler, Surfactant Behavior of Sodium Dodecylsulfate in Deep Eutectic Solvent Choline Chloride/Urea, *Langmuir*, 2015, **31**(47), 12894.
28 A. Sanchez-Fernandez, O. S. Hammond, K. J. Edler, T. Arnold, J. Doutch, R. M. Dalgliesh, P. Li, K. Ma and A. J. Jackson, Counterion binding alters surfactant self-assembly in deep eutectic solvents, *Phys. Chem. Chem. Phys.*, 2018, **20**(20), 13952.
29 J. Ruiz-Olles, P. Slavik, N. K. Whitelaw and D. K. Smith, Self-Assembled Gels Formed in Deep Eutectic Solvents: Supramolecular Eutectogels with High Ionic Conductivity, *Angew. Chem., Int. Ed.*, 2019, **58**(13), 4173.
30 L. Matthews, Ż. Przybyłowicz, S. E. Rogers, P. Bartlett, A. J. Johnson, R. Sochon and W. H. Briscoe, The curious case of SDS self-assembly in glycerol: Formation of a lamellar gel, *J. Colloid Interface Sci.*, 2020, **572**, 384.
31 H. A. Barnes, *A Handbook of Elementary Rheology*, The University of Wales Institute of Non-Newtonian Fluid Mechanics, Aberystwyth, UK, 1st edn, 2000.
32 R. K. Heenan, J. Penfold and S. M. King, SANS at pulsed neutron sources: Present and future prospects, *J. Appl. Crystallogr.*, 1997, **30**, 1140.
33 O. Arnold, J. C. Bilheux, J. M. Borreguero, A. Buts, S. I. Campbell, L. Chapon, M. Doucet, N. Draper, R. Ferraz Leal and M. A. Gigg, *et al.*, Mantid—Data analysis and visualization package for neutron scattering and μ SR experiments, *Nucl. Instrum. Methods Phys. Res., Sect. A*, 2014, **764**, 156.
34 G. D. Wignall and F. S. Bates, Absolute Calibration of Small-Angle Neutron-Scattering Data, *J. Appl. Crystallogr.*, 1987, **20**, 28.
35 J. Berghausen, J. Zipfel, P. Lindner and W. Richtering, Influence of water-soluble polymers on the shear-induced structure formation in lyotropic lamellar phases, *J. Phys. Chem. B*, 2001, **105**(45), 11081.
36 M. Bergstrom, J. S. Pedersen, P. Schurtenberger and S. U. Egelhaaf, Small-angle neutron scattering (SANS) study of vesicles and lamellar sheets formed from mixtures of an anionic and a cationic surfactant, *J. Phys. Chem. B*, 1999, **103**(45), 9888.
37 A. Caille, X-Ray Scattering by Smectic-a Crystals, *C. R. Seances Acad. Sci., Ser. B*, 1972, **274**(14), 891.
38 F. Nallet, R. Laversanne and D. Roux, Modeling X-Ray or Neutron-Scattering Spectra of Lyotropic Lamellar Phases - Interplay between Form and Structure Factors, *J. Phys. II*, 1993, **3**(4), 487.
39 D. F. R. Mildner and P. L. Hall, Small-Angle Scattering from Porous Solids with Fractal Geometry, *J. Phys. D: Appl. Phys.*, 1986, **19**(8), 1535.
40 T. L. Greaves and C. J. Drummond, Ionic liquids as amphiphile self-assembly media, *Chem. Soc. Rev.*, 2008, **37**(8), 1709.
41 C. M. Hansen, Universality of Solubility Parameter, *Ind. Eng. Chem. Prod. Res. Dev.*, 1969, **8**(1), 2.
42 H. S. Salehi, M. Ramdin, O. A. Moultos and T. J. H. Vlugt, Computing solubility parameters of deep eutectic solvents from Molecular Dynamics simulations, *Fluid Phase Equilib.*, 2019, **497**, 10.
43 P. Kekicheff, Phase-Diagram of Sodium Dodecyl-Sulfate Water-System 2. Complementary Isoplethal and Isothermal Phase Studies, *J. Colloid Interface Sci.*, 1989, **131**(1), 133.
44 P. Kekicheff, C. Grabiellemadelmont and M. Ollivon, Phase-Diagram of Sodium Dodecyl-Sulfate Water-System 1. A Calorimetric Study, *J. Colloid Interface Sci.*, 1989, **131**(1), 112.
45 R. A. Abdel-Rahem, Influence of Glycerol and Temperature on the Phase Behavior and Micellization of CTAB and SDS in Aqueous Solutions, *J. Dispersion Sci. Technol.*, 2013, **34**(7), 932.
46 B. Arenas-Gomez, C. Garza, Y. Liu and R. Castillo, Alignment of worm-like micelles at intermediate and high shear rates, *J. Colloid Interface Sci.*, 2020, **560**, 618.
47 J. das Neves, M. V. da Silva, M. P. Goncalves, M. H. Amaral and M. F. Bahia, Rheological properties of vaginal hydrophilic polymer gels, *Curr. Drug Delivery*, 2009, **6**(1), 83.
48 J. Y. Kim, J. Y. Song, E. J. Lee and S. K. Park, Rheological properties and microstructures of Carbopol gel network system, *Colloid Polym. Sci.*, 2003, **281**(7), 614.
49 V. Kobelev and K. S. Schweizer, Dynamic yielding, shear thinning, and stress rheology of polymer-particle suspensions and gels, *J. Chem. Phys.*, 2005, **123**(16), 164903.
50 J. R. Mitchell, The Rheology of Gels, *J. Texture Stud.*, 1980, **11**(4), 315.
51 F. K. Oppong, L. Rubatat, B. J. Frisken, A. E. Bailey and J. R. de Bruyn, Microrheology and structure of a yield-stress polymer gel, *Phys. Rev. E: Stat., Nonlinear, Soft Matter Phys.*, 2006, **73**(4), 041405.
52 H. de Cagny, M. Fazilati, M. Habibi, M. M. Denn and D. Bonn, The yield normal stress, *J. Rheol.*, 2019, **63**(2), 285.
53 J. Y. Lee, J. J. Magda, H. Hu and R. G. Larson, Cone angle effects, radial pressure profile, and second normal stress difference for shear-thickening wormlike micelles, *J. Rheol.*, 2002, **46**(1), 195.
54 T. Shikata, S. J. Dahman and D. S. Pearson, Rheooptical Behavior of Wormlike Micelles, *Langmuir*, 1994, **10**(10), 3470.
55 C. D. Cwalina and N. J. Wagner, Material properties of the shear-thickened state in concentrated near hard-sphere colloidal dispersions, *J. Rheol.*, 2014, **58**(4), 949.
56 Y. F. Lee, Y. Luo, S. C. Brown and N. J. Wagner, Experimental test of a frictional contact model for shear thickening in concentrated colloidal suspensions, *J. Rheol.*, 2020, **64**, 267.

57 T. Chatterjee, M. Linsen, V. V. Ginzburg, D. A. Saucy, A. I. Nakatani and A. K. Van Dyk, Influence of the first normal stress differences on model hydrophobically modified ethoxylated urethane-thickened waterborne paints brush drag, *Prog. Org. Coat.*, 2019, **135**, 582.

58 T. Chatterjee, A. K. Van Dyk, V. V. Ginzburg and A. I. Nakatani, Formulation-Controlled Positive and Negative First Normal Stress Differences in Waterborne Hydrophobically Modified Ethylene Oxide Urethane (HEUR)-Latex Suspensions, *ACS Macro Lett.*, 2017, **6**(7), 716.

59 P. Hebraud, Normal and tangential stress fluctuations during jamming, *Rheol. Acta*, 2009, **48**(8), 845.

60 C. O. Osuji and D. A. Weitz, Highly anisotropic vorticity aligned structures in a shear thickening attractive colloidal system, *Soft Matter*, 2008, **4**(7), 1388.

61 F. C. Mackintosh, J. Kas and P. A. Janmey, Elasticity of Semiflexible Biopolymer Networks, *Phys. Rev. Lett.*, 1995, **75**(24), 4425.

62 B. A. Schubert, E. W. Kaler and N. J. Wagner, The microstructure and rheology of mixed cationic/anionic wormlike micelles, *Langmuir*, 2003, **19**(10), 4079.

63 D. P. Acharya, D. Varade and K. Aramaki, Effect of temperature on the rheology of wormlike micelles in a mixed surfactant system, *J. Colloid Interface Sci.*, 2007, **315**(1), 330.

64 P. A. Hassan, S. J. Candau, F. Kern and C. Manohar, Rheology of wormlike micelles with varying hydrophobicity of the counterion, *Langmuir*, 1998, **14**(21), 6025.

65 R. Kumar, G. C. Kalur, L. Ziserman, D. Danino and S. R. Raghavan, Wormlike micelles of a C22-tailed zwitterionic betaine surfactant: From viscoelastic solutions to elastic gels, *Langmuir*, 2007, **23**(26), 12849.

66 H. Rehage and H. Hoffmann, Viscoelastic Surfactant Solutions – Model Systems for Rheological Research, *Mol. Phys.*, 1991, **74**(5), 933.

67 A. G. Marangoni and S. S. Narine, The influence of microstructure on the macroscopic rheological properties of soft materials, *Scanning*, 1999, **21**(2), 120.

68 P. Wasik, A. M. Seddon, H. Wu and W. H. Briscoe, Dendritic surface patterns from Benard-Marangoni instabilities upon evaporation of a reactive ZnO nanofluid droplet: A fractal dimension analysis, *J. Colloid Interface Sci.*, 2019, **536**, 493.

69 B. B. Mandelbrot, *The fractal geometry of nature*, W. H. Freeman, San Francisco, 1983.

70 P. Bestimmung Scherrer, der Grose und der inneren Struktur von Kolloidteilchen mittels Rontgenstrahlen, *Nachr. Ges. Wiss. Goettingen, Math.-Phys. Kl.*, 1918, 98.

71 A. L. Patterson, The Scherrer formula for X-ray particle size determination, *Phys. Rev.*, 1939, **56**(10), 978.

72 L. Fox, J. Slastanova, A. Taylor, N. Wlodek, M. Bikondoa, O. Richardson and R. M. Briscoe, W. H. Interactions between PAMAM dendrimers and DOPC lipid multilayers: Membrane thinning and structural disorder, *Biochim. Biophys. Acta, Gen. Subj.*, 2021, **1865**, 129542.

73 L. J. Fox, L. Matthews, H. Stockdale, S. Pichai, T. Snow, R. M. Richardson and W. H. Briscoe, Structural changes in lipid mesophases due to intercalation of dendritic polymer nanoparticles: Swollen lamellae, suppressed curvature, and augmented structural disorder, *Acta Biomater.*, 2020, **104**, 198.

74 T. G. Dane, P. T. Cresswell, G. A. Pilkington, S. Lilliu, J. E. Macdonald, S. W. Prescott, O. Bikondoa, C. F. J. Faul and W. H. Briscoe, Oligo(aniline) nanofilms: from molecular architecture to microstructure, *Soft Matter*, 2013, **9**(44), 10501.

75 T. G. Dane, P. T. Cresswell, O. Bikondoa, G. E. Newby, T. Arnold, C. F. J. Faul and W. H. Briscoe, Structured oligo(aniline) nanofilms via ionic self-assembly, *Soft Matter*, 2012, **8**(10), 2824.

76 B. Sironi, T. Snow, C. Redeker, A. Slastanova, O. Bikondoa, T. Arnold, J. Klein and W. H. Briscoe, Structure of lipid multilayers via drop casting of aqueous liposome dispersions, *Soft Matter*, 2016, **12**(17), 3877.

77 R. Guo, M. E. Compo, S. E. Friberg and K. Morris, The coupling action of a hydrotrope and structure transition from lamellar liquid crystal to bicontinuous microemulsion, *J. Dispersion Sci. Technol.*, 1996, **17**(5), 493.

78 P. Kekicheff, B. Cabane and M. Rawiso, Macromolecules Dissolved in a Lamellar Lyotropic Mesophase, *J. Colloid Interface Sci.*, 1984, **102**(1), 51.

79 T.-Y. Chen, E. M. Woo and S. Nagarajan, Periodic Fractal-Growth Branching to Nano-Structured Grating Aggregation in Phthalic Acid, *Sci. Rep.*, 2020, **10**(1), 4062.

80 F. Hausdorff, Dimension and outer dimension, *Mathematische Annalen*, 1919, **79**, 157.

81 C. M. Sorensen, Light scattering by fractal aggregates: A review, *Aerosol Sci. Technol.*, 2001, **35**(2), 648.

82 S. H. Kim Fractal dimensions of a green broccoli and a white cauliflower, arXiv preprint cond-mat/0411597 2004.

83 X. Gu and D. F. R. Mildner, Determination of porosity in anisotropic fractal systems by neutron scattering, *J. Appl. Crystallogr.*, 2018, **51**, 175.

84 J. Teixeira, Small-Angle Scattering by Fractal Systems, *J. Appl. Crystallogr.*, 1988, **21**, 781.

85 K. L. Uahabi and M. Atounti, New approach to the calculation of fractal dimension of the lungs, *Annals of the University of Craiova-Mathematics and Computer Science Series*, 2017, **44**(1), 78.

86 G. B. Ray, I. Chakraborty, S. Ghosh and S. P. Moulik, A critical and comprehensive assessment of interfacial and bulk properties of aqueous binary mixtures of anionic surfactants, sodium dodecylsulfate, and sodium dodecylbenzenesulfonate, *Colloid Polym. Sci.*, 2007, **285**(4), 457.

87 C. Tanford, Micelle Shape and Size, *J. Phys. Chem.*, 1972, **76**(21), 3020.

88 L. Makkonen, A model of hoarfrost formation on a cable, *Cold Reg. Sci. Technol.*, 2013, **85**, 256.

89 W. W. Mullins and R. F. Sekerka, Morphological Stability of a Particle Growing by Diffusion or Heat Flow, *J. Appl. Phys.*, 1963, **34**(2), 323.

90 W. W. Mullins and R. F. Sekerka, Stability of a Planar Interface During Solidification of a Dilute Binary Alloy, *J. Appl. Phys.*, 1964, **35**(2), 444.

91 R. C. Brower, D. A. Kessler, J. Koplik and H. Levine, Geometrical models of interface evolution, *Phys. Rev. A: At., Mol., Opt. Phys.*, 1984, **29**(3), 1335.

92 B. Caroli, C. Caroli and B. Roulet, The Mullins-Sekerka instability in directional solidification of thin samples, *J. Cryst. Grow.*, 1986, **76**(1), 31.
93 J. S. Langer, Instabilities and pattern formation in crystal growth, *Rev. Mod. Phys.*, 1980, **52**(1), 1.
94 P. K. Galenko and D. V. Alexandrov, From atomistic interfaces to dendritic patterns, *Philos. Trans. R. Soc., A*, 2018, **376**(2113), 20170210.
95 H. Brune, C. Romainczyk, H. Röder and K. Kern, Mechanism of the transition from fractal to dendritic growth of surface aggregates, *Nature*, 1994, **369**(6480), 469.
96 Y. Sawada, A. Dougherty and J. P. Gollub, Dendritic and Fractal Patterns in Electrolytic Metal Deposits, *Phys. Rev. Lett.*, 1986, **56**(12), 1260.
97 E. E. Gruber and W. W. Mullins, On the theory of anisotropy of crystalline surface tension, *J. Phys. Chem. Solids*, 1967, **28**(5), 875.
98 S. R. Coriell and R. F. Sekerka, The effect of the anisotropy of surface tension and interface kinetics on morphological stability, *J. Cryst. Grow.*, 1976, **34**(2), 157.
99 G. Radnoczi, T. Vicsek, L. M. Sander and D. Grier, Growth of fractal crystals in amorphous $GeSe_2$ films, *Phys. Rev. A: At., Mol., Opt. Phys.*, 1987, **35**(9), 4012.
100 M. Ambrosi, P. Lo Nostro, L. Fratoni, L. Dei, B. W. Ninham, S. Palma, R. H. Manzo, D. Allemandi and P. Baglioni, Water of hydration in coagels, *Phys. Chem. Chem. Phys.*, 2004, **6**(7), 1401.
101 K. Shinoda, N. Yamaguchi and A. Carlsson, Physical meaning of the Krafft point: observation of melting phenomenon of hydrated solid surfactant at the Krafft point. The, *J. Phys. Chem.*, 1989, **93**(20), 7216.
102 E. Ahmed, J. Breternitz, M. F. Groh and M. Ruck, Ionic liquids as crystallisation media for inorganic materials, *CrystEngComm*, 2012, **14**(15), 4874.
103 J. Potticary, C. Hall, V. Hamilton, J. F. McCabe and S. R. Hall, Crystallization from Volatile Deep Eutectic Solvents, *Cryst. Growth Des.*, 2020, **20**(5), 2877.
104 I. Kapoor, E.-M. Schön, J. Bachl, D. Kühbeck, C. Cativiela, S. Saha, R. Banerjee, S. Roelens, J. J. Marrero-Tellado and D. D. Díaz, Competition between gelation and crystallisation of a peculiar multicomponent liquid system based on ammonium salts, *Soft Matter*, 2012, **8**(12), 3446.
105 D. J. Adams, K. Morris, L. Chen, L. C. Serpell, J. Bacsa and G. M. Day, The delicate balance between gelation and crystallisation: structural and computational investigations, *Soft Matter*, 2010, **6**(17), 4144.
106 P. Dastidar, Supramolecular gelling agents: can they be designed?, *Chem. Soc. Rev.*, 2008, **37**(12), 2699.
107 Y. C. Lin, B. Kachar and R. G. Weiss, Liquid-crystalline solvents as mechanistic probes. Part 37. Novel family of gelators of organic fluids and the structure of their gels, *J. Am. Chem. Soc.*, 1989, **111**(15), 5542.
108 Y. C. Lin and R. G. Weiss, Liquid-crystalline solvents as mechanistic probes. 24. A novel gelator of organic liquids and the properties of its gels, *Macromolecules*, 1987, **20**(2), 414.
109 A. Bot, U. Erle, R. Vreeker and W. G. M. Agterof, Influence of crystallisation conditions on the large deformation rheology of inulin gels, *Food Hydrocolloids*, 2004, **18**(4), 547.
110 G. S. Limiting Manning, Laws and Counterion Condensation in Polyelectrolyte Solutions I. Colligative Properties. The, *J. Chem. Phys.*, 1969, **51**(3), 924.
111 G. S. Manning, Counterion condensation theory constructed from different models, *Phys. A*, 1996, **231**(1), 236.
112 G. S. Manning, Electrostatic free energy of the DNA double helix in counterion condensation theory, *Biophys. Chem.*, 2002, **101–102**, 461.
113 G. S. Manning, Counterion condensation on charged spheres, cylinders, and planes, *J. Phys. Chem. B*, 2007, **111**(29), 8554.
114 A. Faraone, D. V. Wagle, G. A. Baker, E. C. Novak, M. Ohl, D. Reuter, P. Lunkenheimer, A. Loidl and E. Mamontov, Glycerol Hydrogen-Bonding Network Dominates Structure and Collective Dynamics in a Deep Eutectic Solvent, *J. Phys. Chem. B*, 2018, **122**(3), 1261.
115 D. G. Archer and P. Wang, The Dielectric Constant of Water and Debye–Hückel Limiting Law Slopes, *J. Phys. Chem. Ref. Data*, 1990, **19**(2), 371.
116 A. Wolfson, C. Dlugy and Y. Shotland, Glycerol as a green solvent for high product yields and selectivities, *Environ. Chem. Lett.*, 2007, **5**(2), 67.
117 M. O. de la Cruz, L. Belloni, M. Delsanti, J. P. Dalbiez, O. Spalla and M. Drifford, Precipitation of highly charged polyelectrolyte solutions in the presence of multivalent salts, *J. Chem. Phys.*, 1995, **103**(13), 5781.
118 J. A. Schellman and N. Parthasarathy, X-ray diffraction studies on cation-collapsed DNA, *J. Mol. Biol.*, 1984, **175**(3), 313.
119 N. R. Tummala and A. Striolo, Hydrogen-bond dynamics for water confined in carbon tetrachloride-acetone mixtures, *J. Phys. Chem. B*, 2008, **112**(34), 10675.
120 H. Khan, J. M. Seddon, R. V. Law, N. J. Brooks, E. Robles, J. T. Cabral and O. Ces, Effect of glycerol with sodium chloride on the Krafft point of sodium dodecyl sulfate using surface tension, *J. Colloid Interface Sci.*, 2019, **538**, 75.
121 T. Gu and J. Sjöblom, Surfactant structure and its relation to the Krafft point, cloud point and micellization: Some empirical relationships, *Colloids Surf.*, 1992, **64**(1), 39.
122 Y. Moroi, N. Ikeda and R. Matuura, Anionic surfactants with methylviologen or cupric ions as divalent cationic gegenion: Solubility and micelle formation, *J. Colloid Interface Sci.*, 1984, **101**(1), 285.
123 K. Tsujii and J. Mino, Krafft point depression of some zwitterionic surfactants by inorganic salts, *J. Phys. Chem.*, 1978, **82**(14), 1610.
124 K. Tsujii, N. Saito and T. Takeuchi, Krafft points of anionic surfactants and their mixtures with special attention to their applicability in hard water, *J. Phys. Chem.*, 1980, **84**(18), 2287.